



Lymph Node T Cell Homeostasis Relies on Steady State Homing of Dendritic Cells

Meike Wendland,¹ Stefanie Willenzon,¹ Jessica Kocks,¹ Ana Clara Davalos-Misslitz,¹ Swantje I. Hammerschmidt,¹ Kathrin Schumann,² Elisabeth Kremmer,³ Michael Sixt,^{2,5} Angelika Hoffmeyer,⁴ Oliver Pabst,¹ and Reinhold Förster^{1,*}

¹Institute of Immunology, Hannover Medical School, D-30625 Hannover, Germany

DOI 10.1016/j.immuni.2011.10.017

SUMMARY

Little is known about mechanisms determining the homeostasis of lymphocytes within lymphoid organs. Applying different mouse models, including conditionally proficient Ccr7 gene-targeted mice, we now show that semimature steady state dendritic cells (sDCs) constitutively trafficking into lymph nodes (LNs) were essential contributors to T cell homeostasis in these organs. sDCs provided vascular endothelial growth factor known to support high endothelial venule formation, thus facilitating enhanced homing of T cells to LNs. The presence of sDCs led to increased CCL21 production in T-zone fibroblastic reticular cells. CCL21 is a ligand for CCR7 known to regulate homing as well as retention of T cells in LNs. In addition, we provide evidence that CCL21 binds to the surface of DCs via its heparin-binding domain, further explaining why T cells leave LNs more rapidly in the absence of sDCs. Together, these data reveal multiple roles for sDCs in regulating T cell homeostasis in LNs.

INTRODUCTION

Secondary lymphoid organs, such as lymph nodes (LNs), play an important role for the initiation and maintenance of adaptive immune responses. They provide the environment that allows efficient interaction of different subsets of immune cells with each other and with nonhematopoietic stromal cells. The contact of naive T cells with dendritic cells (DCs) presenting antigen in secondary lymphoid organs can serve as a paradigmatic example demonstrating the need for controlled spatiotemporal interaction of cells of the immune system. T cells enter LNs from the blood via specialized high endothelial venules (HEVs) applying a program of sequential adhesion stages including the interaction of T cell-expressed selectins, integrins, and chemokine receptors with their corresponding ligands, which are expressed at the luminal side of HEVs (for recent reviews, see von Andrian and Mackay, 2000; von Andrian and Mempel, 2003). In addition, T cells may arrive

via afferent lymph from LNs located upstream (Braun et al., 2011).

Whereas T cells continuously recirculate between secondary lymphoid organs, immature DCs reside as sentinels in the skin and mucosal surfaces (Banchereau and Steinman, 1998). Therefore, DCs have to be mobilized from peripheral sites and migrate via afferent lymphatics into the draining LN to present antigen to those T cells carrying a cognate antigen receptor. Depending on the nature of the antigen, the maturation status, and the subset of DCs involved, this initial interaction either leads to the induction of tolerance or protective immunity. Immunity is induced by DCs that present antigens derived from pathogens (Steinman et al., 2003), and steady state migratory sDCs presenting self-antigen or innocuous environmental antigens under noninflammatory situations to T cells induce tolerance (Lohr et al., 2005). Data obtained from Ccr7-deficient mice revealed that this chemokine receptor is essential for DC mobilization as well as T cell homing. In Ccr7-deficient mice, LNs and Peyer's patches are poor in T cells and mature DCs and upon adoptive transfer into wildtype recipients, Ccr7-deficient T cells are impaired in homing to LNs (Förster et al., 1999).

Along the same line, DCs differentiated from bone marrow of Ccr7-deficient mice do not migrate to the draining LN after subcutaneous injection or intratracheal instillation (Hintzen et al., 2006; Martin-Fontecha et al., 2003; Ohl et al., 2004). Furthermore, applying in vivo mobilization assays such as fluorescein-isothiocyanate (FITC) skin painting, Ccr7-deficient DCs entirely fail to migrate to the draining LN (Förster et al., 1999). After their intralymphatic injection, Ccr7-deficient T cells and DCs also fail to migrate from their port of entry, the subcapsular sinus, into the T cell area (Braun et al., 2011). Taken together, these data identify CCR7 as a key regulator that control entry of T cells and DCs to LNs. In contrast, the sphingolipid sphingosine-1-phosphate (S1P) and one of its receptors, sphingosin-1phosphate receptor 1 (S1P₁), have been identified as the key molecules that regulate egress of lymphocytes from lymphoid organs. Adoptively transferred S1P₁-deficient T cells accumulate in lymphoid organs and mice deficient for sphingosine kinase, an enzyme that is involved in S1P synthesis, have enlarged LNs (Pappu et al., 2007). Recently, it has been suggested that the balanced expression of CCR7 and S1P1 on T cells as well as the spatial distribution of their cognate ligands regulate the dwell time of T cells within LNs thus contributing to LN homeostasis (Pham et al., 2008).

²Max-Planck-Institute for Biochemistry, D-82152 Martinsried, Germany

³Helmholtz-Zentrum München, Institute of Molecular Immunology, D-81377 Munich, Germany

⁴Nycomed GmbH, D-78467 Konstanz, Germany

⁵Present address: Institute of Science and Technology Austria, A-3400 Klosterneuburg, Austria

^{*}Correspondence: foerster.reinhold@mh-hannover.de



To further dissect the role of CCR7 in LN homeostasis, we generated mice conditionally expressing human CCR7 in a cell type-specific manner. We show that mice expressing human CCR7 in T cells only (T-CCR7+/+ mice) are devoid of LN T cells, although T cells of these mice readily homed to LNs of wildtype recipients after intravenous adoptive transfer. We further observed that LNs of T-CCR7+/+ mice have reduced numbers of HEVs resulting in reduced homing of T cells to LNs. In contrast, mixed bone marrow chimeras possessing hematopoietic cells from WT and T-CCR7+/+ mice as well as mice expressing human CCR7 in T cells and in DCs (DC-T-CCR7+/+ mice) showed normal morphology and T cell counts. We found that DCs produce vascular endothelial growth factor (VEGF) contributing to HEV growth and thus lymphocyte homing. Furthermore, in the presence of DCs, T-zone fibroblastic reticular cells (TRCs) produced increased amounts of CCL21. DCs can bind this chemokine to their cell surface via its heparin-binding domain and thus provide cues that allow T cells to stay for prolonged periods of time within LNs.

RESULTS

Generating Humanized CCR7 Gene-Targeted Mice

To dissect the role of CCR7 on different immune cell populations, we generated a mouse that allows a cell type-specific expression of CCR7. We applied an approach which allowed the induction of human CCR7 instead of the mouse ortholog (Figure S1 available online). This strategy was chosen because mouse CCR7 ligands efficiently induce signals through human CCR7 (Campbell et al., 1998); still, mouse and human CCR7 protein can be distinguished by means of species-specific antibodies.

The strain was designed to disrupt and terminate the murine Ccr7 transcript by insertion of a loxP flanked neomycin (neo) selection cassette and the human CCR7 cDNA (Figure S1) which could not be transcribed as long as the neo cassette was present. These mice could neither express mouse nor human CCR7 (Ccr7-/-CCR7stop/stop). After Cre-mediated recombination, the floxed neomycin cassette was excised to enable the expression of a fusion transcript consisting of the first and second exon of murine Ccr7 fused to an IRES element in front of human CCR7. Translation of this transcript yielded exclusively human CCR7. Notably, human CCR7 was expressed under the control of the endogenous murine Ccr7 promoter and potentially regulatory elements including the murine 3' UTR, which were left intact. This strategy was chosen to ensure that the expression of human CCR7 recapitulates expression of the endogenous mouse Ccr7 gene. Further information regarding the construction of the targeting vector can be found in the Supplemental Information.

We first crossed $Ccr7^{-/-}CCR7^{stop/stop}$ mice to a transgenic strain expressing Cre recombinase ubiquitously in early stages of ontogeny yielding mice carrying human CCR7 alleles in all cell types. The comparative analysis of CD4⁺ cells from peripheral blood of wild-type (Ccr7^{+/+}; WT), heterozygous ($Ccr7^{+/-}$ $CCR7^{+/-}$), and homozygous human CCR7 ($Ccr7^{-/-}CCR7^{+/+}$) mice applying mAb either specific for human or mouse Ccr7 revealed that anti-murine Ccr7 bound to wild-type cells and to cells carrying one allele of both human and murine Ccr7, but failed to bind to cells derived from mice carrying human CCR7 on both

alleles (Figure 1A). Conversely, mAb to human CCR7 neither bound to cells of wild-type mice nor to cells isolated from mice still carrying the *neomycin* resistance gene. However, mice carrying at least one human *CCR7* allele that lacked the *neo* resistance cassette bound anti-human CCR7 (Figure 1A). *Ccr7*^{+/-} *CCR7*^{+/-} mice were further subjected to flow cytometric analysis demonstrating that all cells that expressed mouse Ccr7 also expressed the human ortholog and, vice versa, that human CCR7 was not expressed on cells that lacked expression of mouse Ccr7 (data not shown).

Offspring of chimeric mice was also crossed to C57BL/6 mice for six generations. Applying "speed genomics" parents of the third to fifth generation were selected on the basis of their high degree of C57BL/6 genomic background. F6 mice were then crossed to mice expressing Cre under the control of the *Cd4* promoter giving rise to mice that expressed human CCR7 specifically in T cells (T-*CCR7**/+ mice; Figure 1B).

Together, these results indicate that the mice generated here express human CCR7 instead of the mouse ortholog once the neo cassette has been deleted. For reasons of convenience, mice with two human CCR7 alleles not carrying any neo because of deletion at the germline (GL) level (Ccr7^{-/-}CCR7^{+/+}) will be referred to as GL-CCR7+/+ mice throughout the manuscript. Mice carrying human CCR7 as well as neo on both alleles (Ccr7^{-/-}CCR7^{stop/stop}) will be referred to as CCR7^{stop/stop} mice. Mice generated by intercrossing Ccr7^{-/-}CCR7^{stop/stop} mice with transgenic mice expressing Cre under control of the Cd4 promoter (Ccr7-/-CCR7+/+Cd4-cre+) will be referred to as T-CCR7+/+ mice, whereas mice generated by intercrossing Ccr7^{-/-}CCR7^{stop/stop} mice with Cd4-cre⁺ and Cd11c-cre⁺ (Ccr7^{-/-}CCR7^{+/+}Cd4-cre⁺Cd11c-cre⁺) that express human CCR7 in T cells as well as DCs will be referred to as DC-T-CCR7^{+/+} mice.

Human CCR7 Is Fully Functional in Mice

In transwell migration assays, T cells from GL-CCR7^{+/+} and wild-type mice showed a comparable chemotactic response toward CCL21 whereas T cells from *CCR7*^{stop/stop} mice did not migrate toward this chemokine (Figure 1C). Furthermore, wild-type and GL-CCR7^{+/+} T cells home to the same extent to secondary lymphoid organs of wild-type recipient mice after intravenous injection under competitive in vivo situations (Figure 1D). In addition, FITC skin painting revealed a similar result with regard to homing efficacy. In these experiments, wild-type and GL-CCR7^{+/+} DCs migrated to the same extent to the draining LNs, whereas DCs from *CCR7*^{stop/stop} mice were completely excluded from LNs (Figure 1E).

As observed for GL-CCR7^{+/+} mice, T cells isolated from secondary lymphoid organs of T-CCR7^{+/+} mice migrated as efficiently as wild-type cells toward CCL21 when tested in in vitro transwell migration assays (Figure 1F). The T cell-specific expression of human CCR7 could also be demonstrated functionally, given that DCs of these animals neither migrated in vitro toward CCL21 nor in vivo after FITC skin painting (Figures 1F and 1G).

LNs from wild-type as well as GL-CCR7** mice contained similar numbers of T lymphocytes, whereas LNs of CCR7*stop/stop mice were almost devoid of both CD4* and CD8* T cells (Figure 2A). Accordingly, immunohistology revealed prominent



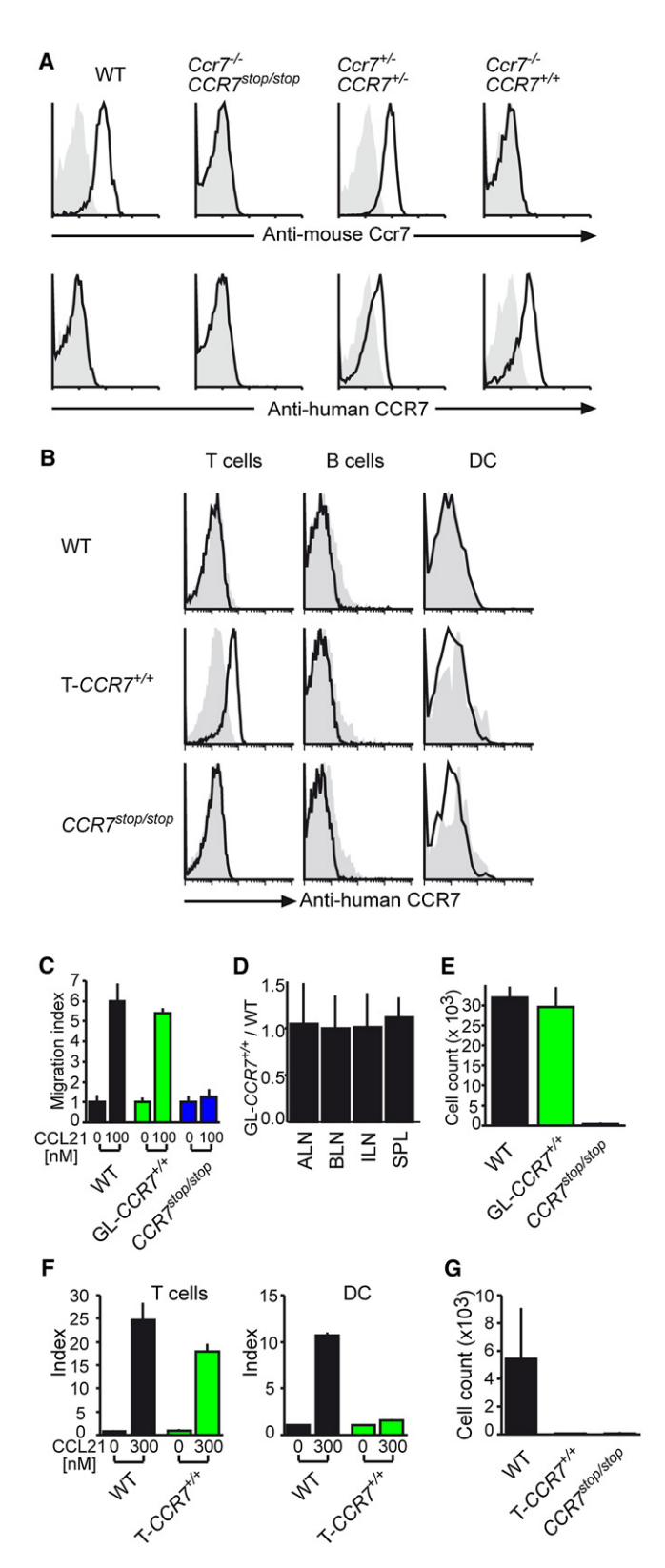


Figure 1. Expression and Functional Analysis of Human and Mouse

(A) Flow cytometry of cells isolated from blood of wild-type (WT), CCR7^{stop/stop} Ccr7+/-CCR7+/-, and GL-CCR7+/+ mice and analyzed for the expression of T cell areas as well as distinct splenic periarteriolar lymphoid sheaths (PALSs) filled with T cells in both wild-type as well as GL-CCR7^{+/+} mice, whereas in CCR7^{stop/stop} mice the paracortex of LNs as well as the splenic PALSs were largely devoid of T cells (Figure 2B). Surprisingly, when analyzing T-CCR7+/+ mice we observed that these mice showed a massive T cell lymphopenia in LNs, which was similar to the one found in CCR7^{stop/stop} mice (Figure 2C), even though T and B cell counts in the peripheral blood were only slightly altered (Figure 2D). Together, these data indicate that the human ortholog of mouse CCR7 is fully functional in mice but that expression of CCR7 on T cells is not sufficient to overcome T cell lymphopenia in LNs.

Reduced Numbers but Fully Functional HEVs in Lymph Nodes of T-CCR7^{+/+} Mice

In order to identify "non-T cell factors" involved in this process, we applied adoptive cell transfers. T cells from wild-type and CCR7stop/stop mice homed at comparable numbers to the spleens of wild-type and T-CCR7+/+ recipients. In contrast, the migration of cells from CCR7^{stop/stop} donors to the peripheral LNs of both recipient strains was impaired as a result of the lack of CCR7 expression (Figure 3A). Interestingly, wild-type T cells homed considerably less efficiently to brachial and inguinal LNs of T-CCR7+/+ mice compared to wild-type recipients, being nearly as inefficient as T cells from CCR7stop/stop donors (Figure 3A). These observations suggest that LNs of T-CCR7^{+/+} mice might not provide the environment required for efficient T cell homing to LNs or for the retention of T cells in these organs.

We thus analyzed the HEVs in LNs of wild-type and T-CCR7+/+ mice. To this end, we stained inguinal LN cryosections with

murine (upper row) or human CCR7 (lower row). Shown are representative results from four independent experiments (see also Figure S1).

(B) Expression of human CCR7 on blood CD4+ T cells, B cells, and spleen CD11c⁺ DCs from WT, T-CCR7^{+/+}, and CCR7^{stop/stop} mice. The shaded areas depict the isotype control.

(C) Chemotaxis of lymphocytes and DCs toward CCL21. Lymphocytes isolated from spleen of WT; (black columns), GL-CCR7+/+ (green columns), and CCR7stop/stop (blue columns) mice were analyzed for their ability to migrate toward CCL21 (0 or 100 nM) within 3 hr (migration index; mean of triplicates + SD of one representative experiment of five performed).

(D) In vivo migration of mouse lymphocytes expressing human CCR7. Lymphocytes isolated from WT and GL-CCR7+/+ mice were labeled with different fluorescent dyes (TAMRA, CFSE) and injected i.v. into WT recipients. After 3 hr, cells were isolated from axillary (ALN), brachial (BLN), and inguinal (ILN) lymph node and spleen (SPL) were stained for CD3 expression. The ratio (+SD) of recovered CD3⁺ of GL- $CCR7^{+/+}$ / WT origin is shown (n = 8 recipients). (E) In vivo FITC skin painting. Both ears of mice with the indicated genotype were painted with FITC solution. Twenty-four hours later, single-cell suspensions of the ear-draining LN were prepared and analyzed by flow cytometry. Shown are absolute cell counts (+SD) of FITC+CD11c+MHCII+ cells (n = 4 mice per group; representative data from one of two experiments performed).

(F) Chemotactic migration of T cells (left) and DCs (right) toward CCL21. T cells isolated from peripheral LNs, and mature BMDCs from WT (black column) or T-CCR7^{+/+} (green column) mice migrated for 3 hr toward medium alone (0) or 300 nM CCL21 (mean +SD; n = 3).

(G) In vivo FITC skin painting of T-CCR7+/+ mice. Animals were painted with FITC solution. Twenty-four hours later, single-cell suspensions of the facial LN of WT, T-CCR7+/+, and CCR7stop/stop mice were analyzed by flow cytometry. Shown are the cell numbers for the recovered $FITC^+CD11c^+MHCII^+$ cells (mean +SD, n = 8 LN of 4 mice/genotype).



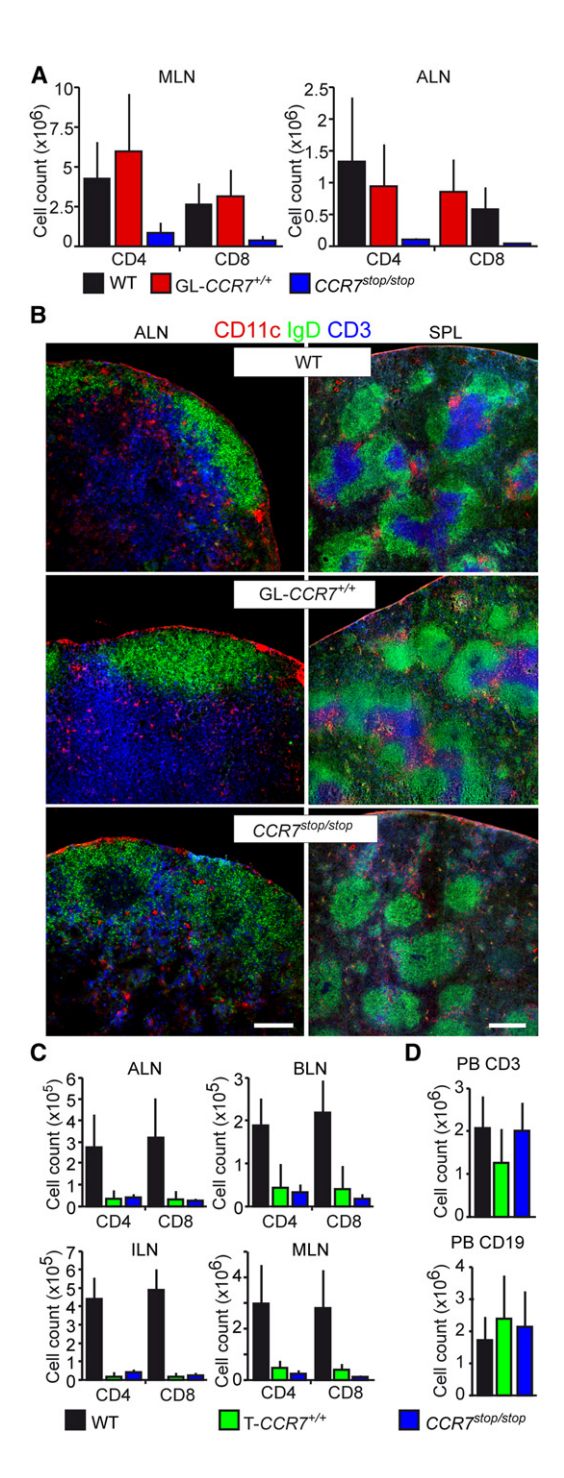


Figure 2. GL-CCR7+/+ Mice Show a WT Phenotype

(A) Distribution of $\mathrm{CD4^{+}}$ and $\mathrm{CD8^{+}}$ T cells in mesenteric and axillary lymph nodes (MLNs and ALNs, respectively). Lymphocytes were isolated from WT (black column), GL-CCR7*/+ (red column), and CCR7*stop/stop (blue column) littermates and stained with antibodies against CD4 and CD8. Absolute cell counts are shown (mean +SD; pooled data from 2 to 8 mice).

(B) Immunohistology of ALN and spleen (SPL) of WT (top), GL-CCR7+/+ (middle), and CCR7^{stop/stop} (bottom) mice. We stained 8 µm cryosections with antibodies indicated. Shown are sections representative for six animals analyzed per genotype.

(C) Distribution of CD4⁺ and CD8⁺ T cells in mesenteric LNs (MLNs), ALNs, BLNs, and ILNs of WT (black columns), T-CCR7+/+ (green columns), and

DAPI, anti-CD31, and MECA79 mAb and analyzed the largest sections of each LN. On the basis of the DAPI staining, we determined the section area morphometrically and found it to be reduced by 30%–40% in T-CCR7 $^{+/+}$ mice (Figure 3B). The determination of the length of all CD31+MECA79+ HEVs present on the entire LN section also demonstrated a ~30% reduction in T-CCR7^{+/+} mice compared to wild-type mice (Figure 3B). However, because we calculated HEV length per mm² section area, we could not see any difference between wild-type and T-CCR7^{+/+} animals, demonstrating that the size reduction of the LNs of T-CCR7+/+ mice is proportional to the reduction in the absolute numbers of HEVs. We next compared the capacity of wild-type and T-CCR7+/+ HEVs to allow homing of wild-type T cells. To this purpose, we transferred red-fluorescent, TAMRA-labeled T cells into wild-type as well as T-CCR7+/+ recipients. Mice were sacrificed 30 min later; cyrosections of their inguinal LNs were stained with MECA79 mAb. The number and position of the adoptively transferred cells relative to HEVs was analyzed. With regard to the location of the adoptively transferred cells, five different positions were determined: (1) within the lumen of a HEV; (2) attached to the luminal site of the HEVs; (3) within HEVs; (4) at the abluminal site of the HEVs; and (5) within tissue (Figure 3C). With the exception of cells located within the HEV lumen, we found significantly more adoptively transferred cells per entire LN section in wild-type recipients at all sites analyzed (Figure 3D). However, we could not find any significant difference between wild-type and T-CCR7^{+/+} recipients once numbers of homed cells were calculated per section area unit (Figure 3E). Collectively, these findings show that LNs of T-CCR7+/+ mice have less HEVs than LNs of wild-type mice but suggest that these HEVs are functional.

DC Migration and Lymph Node T Cell Homeostasis

To test the idea that lack of sDCs in T-CCR7+/+ mice might contribute to the observed LN lymphopenia, we subcutaneously injected TAMRA-labeled semimature wild-type bone marrowderived dendritic cells (BMDCs) into the left foot pad and PBS into the right foot pad of T-CCR7+/+ mice. After 5 days, mice were sacrificed and popliteal LNs (popLNs) were analyzed by immunohistology. Compared to PBS-draining LNs, DC-draining LNs showed a strong increase in size (Figures 4A and 4C). The LN that received the transferred DCs also showed a regularly developed paracortex full of T cells in contrast to LNs draining the applied PBS (Figure 4A). Additionally, DC-draining LNs showed increased numbers of MECA79+ HEVs (Figures 4B and 4D), indicating that trafficking of sDCs from the periphery contributed to HEV development. Further analysis revealed a high correlation between LN cellularity and the number of adoptively transferred semimature DCs reaching the popLNs (Figure 4E). Furthermore, DC-draining popLN displayed a ~3fold increase in VEGF levels compared to PBS-draining LNs,

CCR7^{stop/stop} (blue columns) mice. Absolute cell counts were determined for CD4+ and CD8+ T cells (mean + SD; n = 3 mice/genotype; shown is one representative experiment of four experiments performed).

(D) Distribution of CD3+ and CD19+ cells in peripheral blood (PB) of WT, T-CCR7^{+/+}, and CCR7^{stop/stop} mice as indicated (mean + SD, n = 5 to 29 mice/



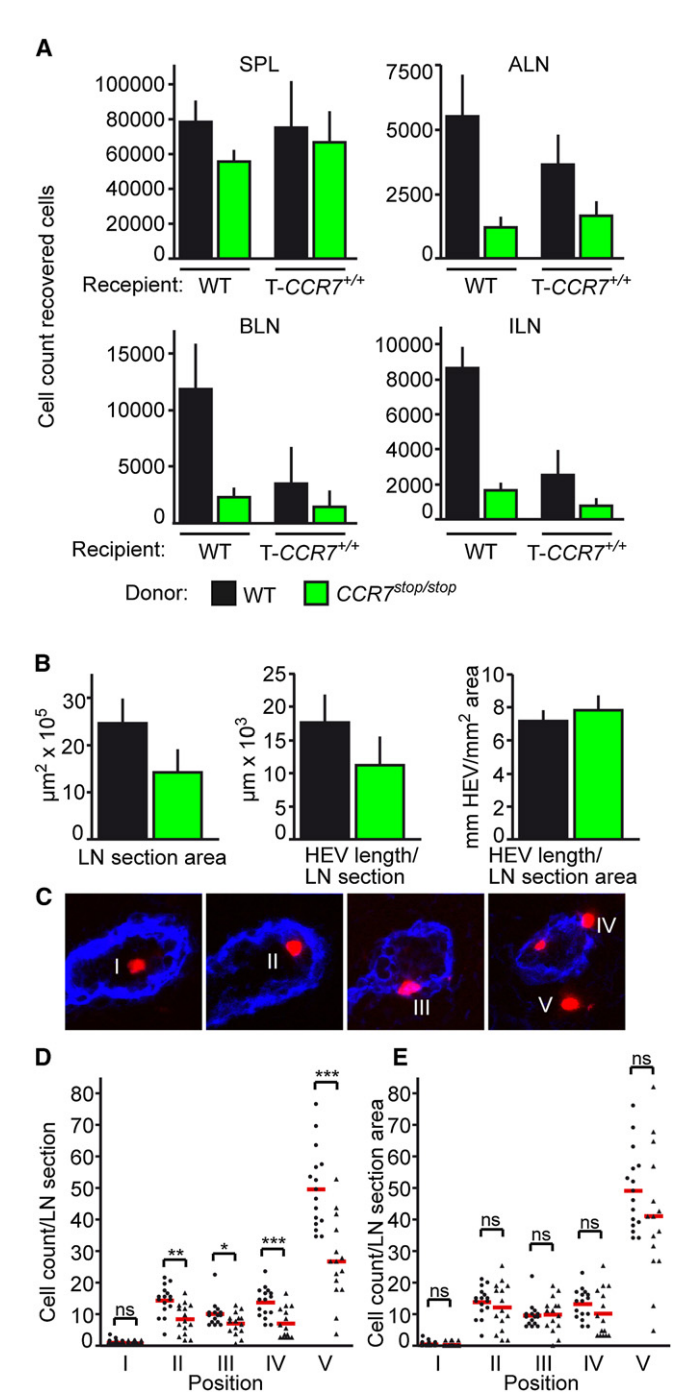


Figure 3. Reduced Homing of WT T Cells to T-CCR7*/+ Recipients
(A) Cells isolated from LNs and spleens of WT (black columns) and CCR7*stop/stop
(green columns) mice were labeled with TAMRA and CFSE, respectively.
Labeled cells were i.v. transferred to WT or T-CCR7*/+ recipients as indicated.
Three hours after injection, the mice were sacrificed and lymphocytes were
isolated from SPL, ALNs, BLNs, and ILNs to recover transferred cells. Absolute
cell count of recovered CD3* lymphocytes are shown (mean +SD; n = 4
recipients/group).

(B) Measurement of high endothelial venule (HEV) length and LN section area in WT (black columns) and T- $CCR7^{+/+}$ (green columns) mice. ILN cryosections were stained with anti-CD31 and Meca79 mAb and DAPI and analyzed by fluorescent microscopy and morphometry. On the basis of DAPI staining, the LN section area (left panel) has been determined. The length (μ m) of the HEVs

as detected by ELISA (Figure 4F). To demonstrate that the DCs themselves were a source of VEGF, we tested their capacity to secrete VEGF. ELISA revealed that 100,000 semimature BMDCs produced $\sim\!10$ pg VEGF in 24 hr (data not shown). Furthermore, qRT-PCR on T cells and DCs isolated by flow sorting from peripheral LNs of C57BL/6 mice confirmed that DCs were a relevant source of VEGF (Figure 4G). To further confirm the idea that sDC contribute to LN homing, we s.c. injected semimature BMDCs or PBS in the hind flank of mice. After 5 days, these mice i.v. received TAMRA-labeled T cells from wild-type donors for 3 hr. The s.c. transfer of DCs led to a $\sim\!4$ -fold increase in short-term homing of T cells. Together, these data suggest that the migration of DCs to LNs contribute to HEV formation and efficient homing of T cells (Figure 4H).

Rag2-Deficient Bone Marrow Chimeras Rescue the Phenotype of T-CCR7*/* Mice

To further address the role of steady state DC migration on LN T cell homeostasis, we generated $Rag2^{-/-} + T\text{-}CCR7^{+/+} \rightarrow T\text{-}CCR7^{+/+}$ bone marrow chimeras. To this end, we lethally irradiated $T\text{-}CCR7^{+/+}$ mice and reconstituted them with either $T\text{-}CCR7^{+/+}$ bone marrow ($T\text{-}CCR7^{+/+} \rightarrow T\text{-}CCR7^{+/+}$) or a mixture of 20% $T\text{-}CCR7^{+/+}$ and 80% $Rag2^{-/-}$ bone marrow ($T\text{-}CCR7^{+/+} + Rag2^{-/-} \rightarrow T\text{-}CCR7^{+/+}$). All lymphocytes present in the latter mice are of $T\text{-}CCR7^{+/+}$ origin, whereas a considerable part of the nonlymphoid hematopoietic cells, including DCs, are derived from $Rag2^{-/-}$ progenitors, thus carrying both mouse Ccr7 alleles.

Analyzing bone marrow chimeras 8 weeks after reconstitution, we found that LNs of T- $CCR7^{+/+}$ + $Rag2^{-/-}$ \rightarrow T- $CCR7^{+/+}$ chimeras contained increased numbers of CD11c+MHCIIhigh cells compared to T- $CCR7^{+/+}$ \rightarrow T- $CCR7^{+/+}$ mice. Interestingly, in contrast to the T- $CCR7^{+/+}$ \rightarrow T- $CCR7^{+/+}$ chimeras, the vast majority of DCs present in the T- $CCR7^{+/+}$ + $Rag2^{-/-}$ \rightarrow T- $CCR7^{+/+}$ chimeras expressed mouse CCR7 (Figure 5A). Furthermore, immunohistology revealed that LN paracortices in T- $CCR7^{+/+}$ + $Rag2^{-/-}$ \rightarrow T- $CCR7^{+/+}$ chimeras were filled with T cells, whereas the corresponding area in LNs of T- $CCR7^{+/+}$ \rightarrow T- $CCR7^{+/+}$ mice were largely devoid of T cells (Figure 5B). A flow cytometry-based analysis of LNs confirmed strongly increased T cell counts in T- $CCR7^{+/+}$ + $Rag2^{-/-}$ \rightarrow T- $CCR7^{+/+}$ chimeras (Figure 5C).

On the basis of the observation that the paracortex of LNs from T-CCR7 $^{+/+}$ + Rag2 $^{-/-}$ \to T-CCR7 $^{+/+}$ chimeras was filled with

has been determined on the basis of CD31 $^+$ Meca79 $^+$ endothelial cells (middle panel). The right panel indicates the length of the HEVs in relation to the section area of the LN (mean + SD; n = 16 section derived from 8 ILNs per group). (C) Adoptive transfer of WT T cells in WT and T- $CCR7^{+/+}$ mice. Lymphocytes were isolated from peripheral LNs and spleen of WT mice, pooled, and MACS-sorted for T cells. After labeling with TAMRA, T cells were injected into the tail vein for 30 min. We stained 8 μ m cryosections of the ILN of recipients with anti-CD31 and Meca79 mAb. The micrographs display the positions (I–V) of labeled T cell that were analyzed in (D): (I) inside HEV without obvious contact to endothelial cells; (II) attached to the luminal surface of HEV; (III) between HEV endothelial cells; (IV) attached to the abluminal surface of HEV; and (V) in the LN without obvious contact to HEV.

(D and E) Cell counts of transferred T cells in ILNs of WT (dots) and T- $CCR7^{*/*}$ (triangles). Cell counts of transferred T cells are shown per LN section (D) or per LN section area (E, dots and triangles indicate individual sections, and red bars mean values obtained from 16 sections of 8 ILN per genotype).



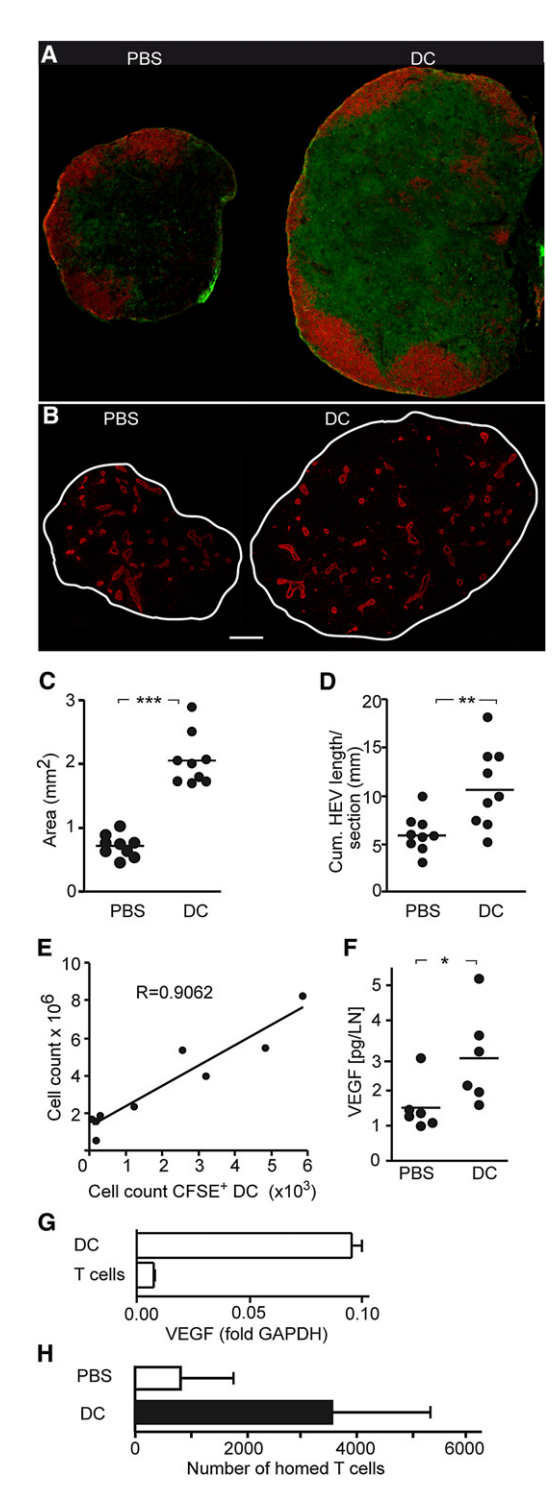


Figure 4. DCs Express VEGF and Induce HEV Growth

(A and B) Semimature BMDCs were injected s.c. into the right and PBS into the left flank and footpad of T- $CCR7^{+/+}$ mice. Immunohistology of popLNs of T- $CCR7^{+/+}$ mice 5 days after s.c. injection of semimature BMDCs into the footpad. We stained 8 μ m cryosections of 6- to 8-week-old mice with antibodies against CD3 (green) and B220 (red; A) or MECA79 (B). Shown are sections representative for nine LNs analyzed per group.

(C) Analysis of the section area of popLNs in T-CCR7^{+/+} mice 5 days after s.c. injection of PBS or semimature BMDCs into the footpad. Dots indicate LNs from nine mice; red bars indicate mean values.

T cells, we speculated that the continuous homing of DCs to LNs not only might affect T cell homing but also the LN dwell time of T cells. To test this hypothesis, we aimed to address how fast T cells leave skin-draining LNs of wild-type and T-CCR7^{+/+} mice. To that end, we TAMRA-labeled pooled lymphocytes from wild-type spleen and LNs, which contained ~45% T cells, and adoptively transferred them to wild-type and T-CCR7+/+ recipients. After 20 hr, half of the animals of each group were sacrificed, and the remaining recipients i.v. and i.p. received anti-L-selectin antibodies (MEL-14) for preventing further homing of recirculating lymphocytes before they were analyzed 14 hr later. We found that, before applying the anti-L-selectin mAb, 78.7% ± 6.0% of the transferred cells homing to wildtype LNs were T cells. After anti-L-selectin mAb treatment, this value slightly decreased to 72.0% ± 11.7%. In contrast, in LNs of T-CCR7^{+/+} mice, the frequency of T cells within the transferred cells dropped from 64.2% $\pm 7.6\%$ before to 35.8% \pm 9.0% after anti-L-selectin treatment (Figure 5D; mean ± SD; n = 35 LNs of 7 animals per group analyzed in two independent experiments). Together, these findings indicate that under steady state condition, T cells are less efficiently retained in the LNs of T-CCR7+/+ mice compared to wild-type mice.

Increased CCL21 Levels in Lymph Nodes of T-CCR7*/+ + Rag2-/- Chimeras

On the basis of the above described results and because of the observation that T cells accumulate in the T cell zone of T- $CCR7^{+/+} + Rag2^{-/-} \rightarrow T$ - $CCR7^{+/+}$ chimeras, we speculated that non-T cell factors might be responsible for the reduced dwell time observed in T-CCR7+/+ mice. Given that Ccr7 expression on T cells has recently be described to affect their retention in LNs (Pham et al., 2008), we analyzed the expression of CCL21 in the above described T-CCR7^{+/+} + $Rag2^{-/-} \rightarrow T$ -CCR7^{+/+} and T-CCR7^{+/+} → T-CCR7^{+/+} chimeras. Staining cryosections with anti-CCL21, we observed in both experimental groups expression of CCL21 in HEVs and cells within the T cell areas. However, the staining of CCL21 on cells within the T cell area was apparently brighter in T-CCR7^{+/+} + Rag2^{-/-} \rightarrow T-CCR7^{+/+} chimeras compared to the T- $CCR7^{+/+} \rightarrow T-CCR7^{+/+}$ chimeras (Figure 5E). A quantitative morphometric expression analysis over the LN sections confirmed a 2-fold increase of CCL21 expression per

⁽D) Measurement of high endothelial venule (HEV) length in popLNs of T-CCR7*/+ 5 days after s.c. injection of PBS or semimature BMDCs into the footpad. HEV length has been determined as described in Figure 3B. Dots indicate LNs from nine mice; red bars indicate mean value.

⁽E) Semimature BMDCs were labeled with CFSE and then injected s.c. in the flank and footpad of T-CCR7*/+ mice. After 5 days, the cellularity of the draining LNs has been determined and correlated to the number of homed DCs. "R" indicates the correlation constant. Dots indicate individual LNs. (F) popLNs from T-CCR7*/+ mice receiving PBS or DCs s.c. into the footpad

⁽F) popLNs from T-CCR7*/+ mice receiving PBS or DCs s.c. into the footpad were harvested at day 5 and analyzed for the expression of VEGF with ELISA. Dots indicate individual LNs.

⁽G) DCs and T cells were sorted from LN by flow cytometry and analyzed by qRT-PCR for the expression of VEGF-A (mean +SD; n=4; data were derived from at least two independent experiments).

⁽H) *Ccr7*-deficient mice were injected s.c. with PBS or 2×10^6 WT BMDCs. After 5 days, T cells were isolated from WT donors, labeled with TAMRA, and i.v. transferred (5.8 \times 10⁶). After 3 hr, recipients were sacrificed and the number of TAMRA⁺ cells was determined in the ingLNs (mean +SD, n = 4–5 mice/per group from two independent experiments).



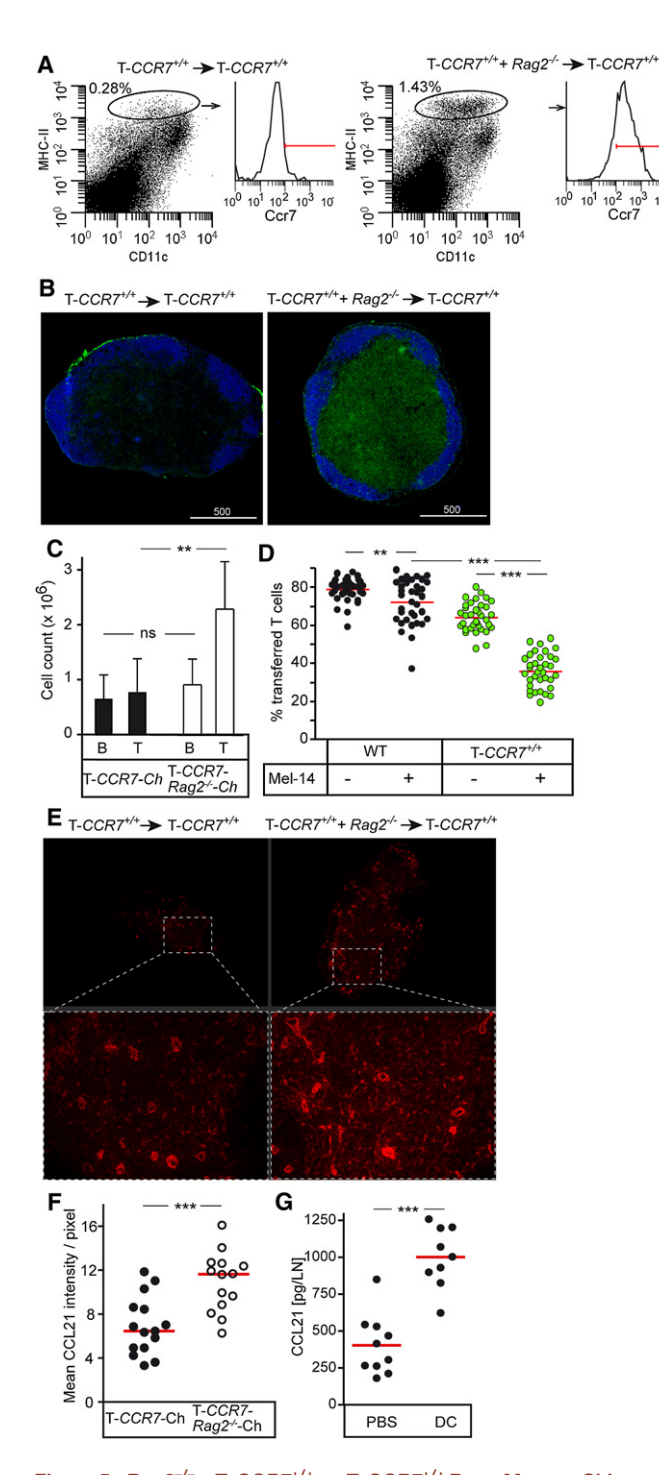


Figure 5. Rag2^{-/-} + T-CCR7^{+/+} → T-CCR7^{+/+} Bone Marrow Chimeras Show Filled T Cell Areas and Increased Expression of CCL21

(A) Flow cytometry of cells isolated from peripheral LNs of T-CCR7+/+ -T-CCR7^{+/+} chimeras (left) and $Rag2^{-/-}$ + T-CCR7^{+/+} \rightarrow T-CCR7^{+/+} (right) chimeras. The expression of human CCR7 is shown for MHC-II+ CD11c+ cells. (B) Immunohistology of peripheral LN of T-CCR7^{+/+} → T-CCR7^{+/+} (left) and $Rag2^{-/-}$ + T-CCR7^{+/+} \rightarrow T-CCR7^{+/+} mice. We stained 8 μm cryosections with antibodies against CD3 (green) and B220 (blue).

(C) B and T cell counts (mean + SD) of lymphocytes isolated from peripheral LNs of T-CCR7 $^{+/+}$ \rightarrow T-CCR7 $^{+/+}$ mice (T-CCR7-Ch, filled column) and $Rag2^{-/-}$ + T-CCR7^{+/+} \rightarrow T-CCR7^{+/+} chimeras (T-CCR7-Rag2^{-/-}-Ch, open column). In (A)–(C), data of n = 10 and 20 LNs.

pixel in T-CCR7^{+/+} + Rag2^{-/-} \rightarrow T-CCR7^{+/+} chimeras (Figure 5F). Because LNs of T-CCR7 $^{+/+}$ + Rag2 $^{-/-}$ \rightarrow T-CCR7 $^{+/+}$ mice harbor skin-derived DCs, we hypothesized that these cells might have contributed to the increased CCL21 levels observed in the chimeric LNs, even though mouse DCs do not express CCL21 by themselves (Link et al., 2007). Analysis of the draining LNs of T-CCR7+/+ mice that s.c. received semimature DCs or PBS 4 days earlier revealed a more than 2-fold increase in the levels of CCL21 per LN in the group that received the DCs (Figure 5G). These results indicate that the presence of DCs might enhance the production of CCL21 in LNs.

Expression of CCR7 on T Cells and DCs Restores LN Homeostasis

The T-CCR7^{+/+} + Rag2^{-/-} \rightarrow T-CCR7^{+/+} chimeras did not restore CCR7 selectively on DCs but potentially also on other cells. To overcome this limitation, we crossed Cd11c-cre+ mice to the T-CCR7+/+ mice, which led to the generation of mice expressing human CCR7 on T cells as well as DCs but not on B cells (DC-T-CCR7+/+ mice; Figure 6A). Human CCR7 was also not expressed on plasmacytoid (p)DCs but slightly expressed on lymphoid tissue inducer (LTi) cells (Figures S2A and S2C) but both populations were surprisingly slightly reduced in LNs of DC-T-CCR7*/+ mice (Figures S2B and S2D). Analysis of skin-draining LNs revealed that T cells as well as DCs were strongly diminished in number in T-CCR7+/+ mice, whereas they were present at comparable numbers in the LNs of DC-T-CCR7^{+/+} and wild-type mice. We also observed some reduction of B cells in T-CCR7^{+/+} mice but regular counts in DC-T-CCR7^{+/+} animals, suggesting that the presence of DCs, either directly or indirectly, possibly by increasing the T cell numbers within LNs, might also have some effect on LN B cell homeostasis (Figure 6B). Immunohistology revealed regular morphology of LNs and spleen of DC-T-CCR7+/+ mice with large numbers of T cells and DCs residing in LN paracortex and the splenic white pulp, respectively (Figure 6C).

The main source of CCL21 within LNs are TRCs, but these cells rapidly lose the capacity to produce this chemokine once they are removed from their natural environment and being cultured in vitro (Link et al., 2007). To test whether DCs contribute to expression of CCL21 by TRCs, we isolated TRCs from wild-type, CCR7^{stop/stop}, T-CCR7^{+/+}, and DC-T-CCR7^{+/+}

(D) Egress of lymphocytes in the peripheral LNs of WT and T-CCR7^{+/+} mice. TAMRA-labeled WT cells were transferred to WT and T-CCR7+/+ mice. Twenty hour later, one part of the mice was sacrificed while the other part was treated with the L-selectin blocking antibody Mel 14. Another 14 hr later, treated mice were sacrificed. Lymphocytes were isolated from peripheral LNs and analyzed by flow cytometry. The panel shows the percentage of CD3⁺ cells within the transferred cells of antibody treated and untreated WT and T-CCR7+/+ mice (7 mice with n = 35 LNs analyzed per group in two independent experiments; dots show represent individual LNs).

(E) Analysis of CCL21 expression in peripheral LNs of T-CCR7 $^{+/+}$ \rightarrow T-CCR7^{+/+} and $Rag2^{-/-}$ + T-CCR7^{+/+} \rightarrow T-CCR7^{+/+} chimeras. Crysections were stained and analyzed for the expression of CCL21 (red).

(F) The panel indicates the mean of CCL21 intensity per pixel of LN cryosection of T-CCR7 $^{+/+}$ \rightarrow T-CCR7 $^{+/+}$ mice (T-CCR7-Ch, filled circles) and Rag2 $^{-/-}$ + T- $CCR7^{+/+} \rightarrow T$ - $CCR7^{+/+}$ chimeras (T-CCR7- $Rag2^{-/-}$ -Ch, open circles). Each circle represents the intensity per pixel of one LN cryosection.

(G) The amount of CCL21 present in the inguinal LN of T-CCR7 $^{+/+}$ mice 5 days after the s.c. footpad injection of PBS or DCs.



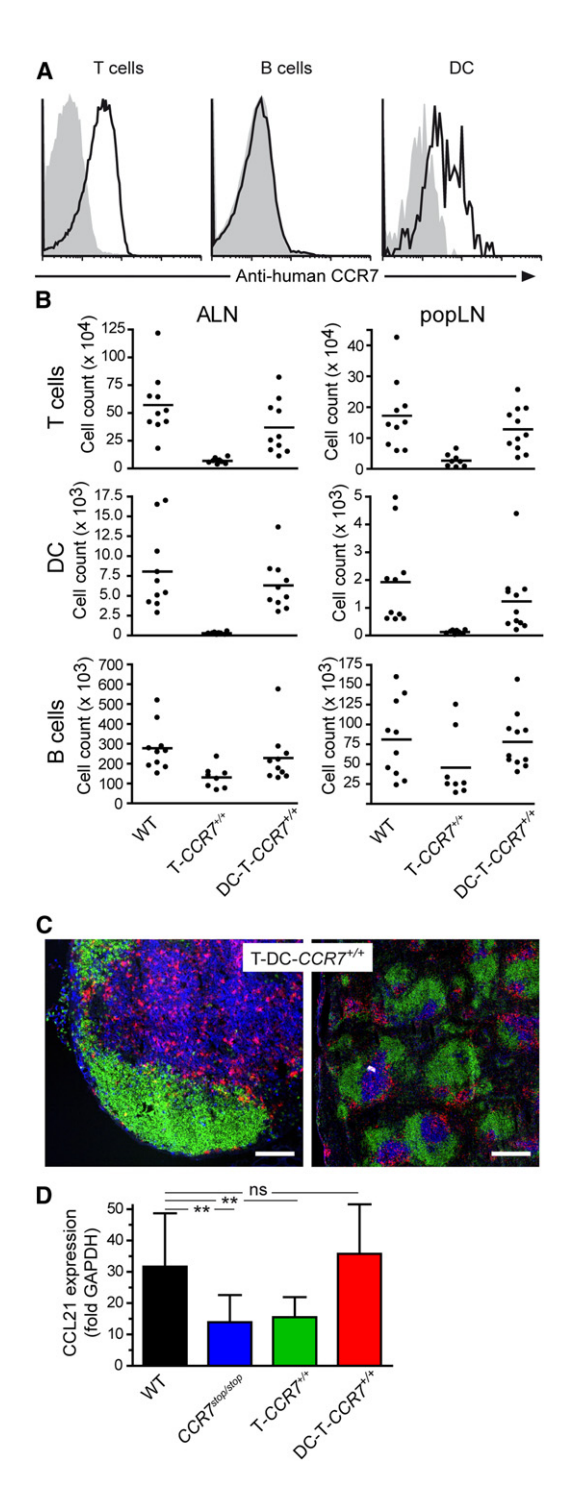


Figure 6. Mice Expressing CCR7 on DCs and T Cells Show a Regular Phenotype

(A) Expression of human CCR7 on T cells, B cells, and DCs isolated from LNs of DC-T- $CCR7^{+/+}$ mice.

(B) Quantitative analysis of T cells (CD3+B220-), DCs (CD11c+ MHC II high), and B cells (B220+CD3-) in ALN and popLN of WT, T-CCR7+/+ and DC-T-CCR7+/+ mice as indicated (dots represent individual mice, pooled data derived from three to four independent experiments).

(C) Immunohistology of cryosections of LN (left) and spleen (right) from DC-T-CCR7*/+ mice; green, anti-B220; blue, anti-CD3; red, anti-CD11c; representative data of more than 5 animals analyzed).

mice and determined CCL21 expression relative to GAPDH by qRT-PCR. Interestingly, TRCs isolated from DC-T-CCR7*-/- mice expressed CCL21 at similar levels to those isolated from wild-type LNs, whereas the expression of CCL21 by TRCs isolated from both $CCR7^{stop/stop}$ and T- $CCR7^{+/+}$ mice was reduced to $\sim\!50\%$ of the wild-type levels (Figure 6D). Collectively, these data indicate that expression of CCR7 on DCs is essential for T cell homeostasis in LNs and that steady state-trafficking DCs contribute to some degree to CCL21 expression in these organs.

DCs Bind Stromal Cell-Derived CCL21

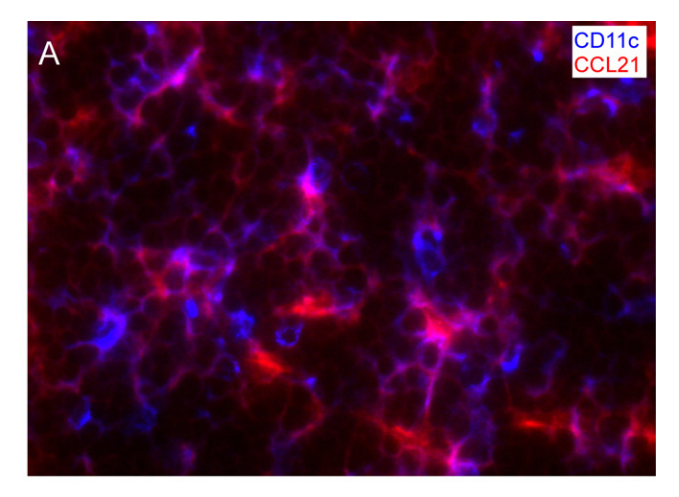
As mentioned before, mouse DCs do not express CCL21 (Link et al., 2007). Still we detected high amounts of CCL21 in the T cell area of T-CCR7^{+/+} + Rag2^{-/-} \rightarrow T-CCR7^{+/+} chimeras. We therefore tested whether DCs in lymphoid organs not only contribute to CCL21 production by TRCs but also bind this chemokine, leading to its retention within LNs. Indeed, immunohistology of LN sections from untreated wild-type mice revealed costaining of CD11c and CCL21 (Figure 7A), indicating that DCs bind CCL21 as described by others before (Friedman et al., 2006). Furthermore, DCs isolated from peripheral LNs from wild-type but not from plt/plt mice carried CCL21 on their cell surface as revealed by flow cytometry (Figure 7B). Incubating BMDCs from wild-type and Ccr7-deficient mice with different concentrations of recombinant CCL21 and then staining them with anti-CCL21 revealed that BMDCs strongly bind CCL21 and that this binding to a large degree did not occur via binding to CCR7 because it was also observed on Ccr7-deficient DCs (Figure 7C and data not shown). However, preincubation of CCL21 with different concentrations of Heparin before or at the time of DC staining completely interfered with the binding of CCL21 to DCs (Figure 7C and data not shown). This suggests that DCs bind CCL21 via its heparin-binding domain. To experimentally address whether CCL21 binds to sulphated proteoglycans on the surface of DCs, we differentiated BMDCs in the presence of NaClO₃, which inhibits chondroitin and heparan sulfation (Humphries and Silbert, 1988). Indeed, the addition of NaClO₃ to the culture medium for the last 3 days of differentiation prevented the binding of exogenously added CCL21 to DCs (Figure 7D). Together with the Heparin blocking experiments, these data strongly suggest that CCL21 efficiently binds to DCs via its heparin-binding domain.

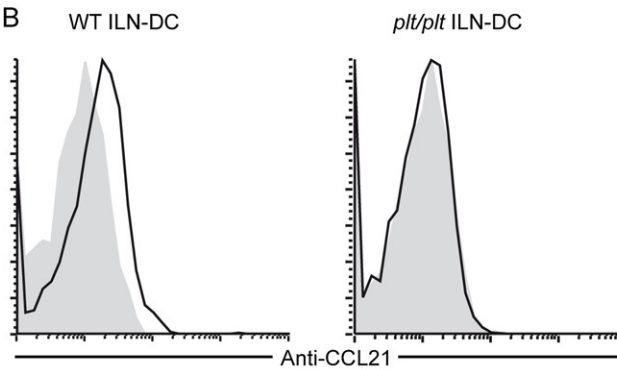
DISCUSSION

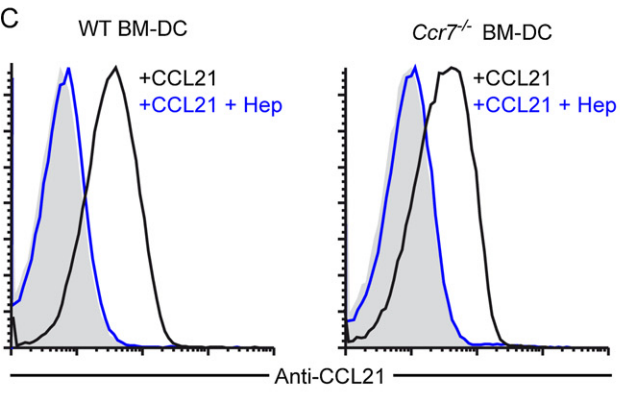
The importance of continuous afferent lymph flow for LN homeostasis has been shown earlier by Mebius et al. (1991). Data from the present study indicate that a CCR7-dependent steady state migration of DCs into LNs is a key event for the maintenance of unperturbed LN T cell homeostasis. We provide evidence that steady sDCs reaching LNs via the afferent lymph are involved at least in three different processes that contribute to LN T cell homeostasis. sDCs (1) produce VEGF, which is known to act

(D) TRCs were isolated by flow cytometry from mice with the genotype indicated and assessed by qRT-PCR for the expression of CCL21 relative to GAPDH (mean +SD, pooled data from multiple qRT-PCR runs with mRNA isolated from 4 independent experiments).









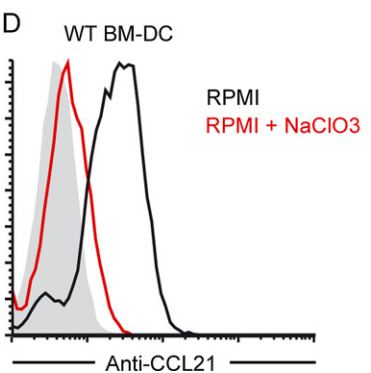


Figure 7. DCs "Present" CCL21 on Their Surface

(A) Colocalization of CD11c and CCL21 on cryosections from LNs of C57BL/6 mice.

(B) Cells isolated from the inguinal LNs of wild-type or *plt/plt* mice were stained with anti-MHCII-FITC, anti-CD11c-APC, and anti-CCL21/donkey-anti-goat-bio/streptavidin-PerCP. Shown is CCL21 expression of CD11c⁺MHCII⁺ cells. (C) WT or *Ccr7*-deficient bone marrow derived DCs were incubated with 2.5 μg/ml CCL21 (black line) alone or together with 1.25 U heparin (blue line). After extensive washing, binding of CCL21 to DCs was revealed by flow cytometry applying CCL21 antibodies.

(D) WT BMDCs were differentiated in vitro in the absence (black line) or presence of NaClO₃ (red line) for the last 3 days of culture. DCs were incubated with CCL21 and stained for CCL21 binding as described for (C). Solid lines represent CCL21 staining on DCs. Gray areas represent the control. Shown are representative results from at least three independent experiments.

as a growth and differentiation factor for HEVs thus allowing the efficient homing of T cells to LNs, (2) support CCL21 expression by TRCs, and (3) bind CCL21 produced by TRCs, thereby providing retention signals that prolong the dwell of T cells within LNs.

Although it has been well established that different classes of adhesion molecules are essentially involved in LN homing (Sackstein, 2005; von Andrian and Mempel, 2003), little is known about factors that control lymphocyte egress. On the basis of gene-targeting in mice, sphingosin-1-phosphate receptor 1 (S1P₁) has been identified as a key regulator of lymphocyte egress (Cyster, 2005; Rosen et al., 2007). As a mode of action, it seems that LN egress might reflect a S1P1-mediated chemotactic response of T cells toward high levels of S1P present in the efferent lymph fluid within medullary or cortical sinuses. From the observation that Ccr7-deficient T cells egress more efficiently from LNs than wild-type T cells, it has been suggested that S1P-egresspromoting signals are counteracted by CCL21 expressed by TRCs (Pham et al., 2008). Data from the present study support and extend this model: We show that LNs of a conditional T-CCR7^{+/+} proficient strain are lymphopenic probably as a result of reduced levels of CCL21 present in the T cell zone, which in turn is owed to impaired steady state migrating DCs, not only supporting TRCs to express CCL21 but also contributing to present CCL21 to T cells. Considering the fact that DCs build a dense network within the T cell zone it seems plausible that DCs substantially increase the area for CCL21 trapping and presentation.

Although we cannot formally exclude the possibility that human CCR7 might not work exactly as murine Ccr7 in mice, data obtained from the GL- $CCR7^{+/+}$ mice strongly indicate that human CCR7 can fully substitute for Ccr7 deficiency. Therefore, it was unexpected to see that the T- $CCR7^{+/+}$ mice have strongly reduced LN T cell counts. Adoptive transfers revealed that considerably less wild-type donor cells were present in T- $CCR7^{+/+}$ recipients than in wild-type recipients 3 hr after transfer indicating that non-T cell factors might cause LN T cell lymphopenia in T- $CCR7^{+/+}$ mice. The LNs of the latter animals have $\sim 30\%$ to 40% less HEVs. Despite of the reduced numbers of HEVs observed in the LNs of T- $CCR7^{+/+}$ mice, short-term adoptive transfers of wild-type donor cells in wild-type and T- $CCR7^{+/+}$ mice suggest that those HEVs present seem to be fully functional.

Under inflammatory conditions, DCs have been identified as a source for VEGF that triggers vascular growth, including



proliferation of HEV endothelial cells, an event that is associated with increased lymphocyte entry into LNs (Webster et al., 2006). Data from the present study indicates that also in the steady state, DCs directly contribute to HEV growth. After subcutaneous injection of cluster-disrupted semimature BMDCs, which produce VEGF to relevant amounts, into T-CCR7*/+ recipients we observed increased numbers of HEV endothelial cells and increased VEGF expression in the draining LNs. Furthermore, we detected considerable VEGF production by DCs isolated from untreated LNs. However it seems also possible that DCs might have indirect effects on HEV growth via interactions with TRCs, which are a known source of VEGF (Chyou et al., 2008).

In addition to their effect on HEVs, several lines of evidence from the present study support the idea that sDCs also affect the dwell time naive T cells stay within a LN: (1) In contrast to T- $CCR7^{+/+} \rightarrow T$ - $CCR7^{+/+}$ chimeras, T- $CCR7^{+/+} + Rag2^{-/-} \rightarrow$ $T\text{-}CCR7^{+/+}$ chimeras not only possess regular frequencies of LN DCs but also a 3-fold increase in T cell numbers. (2) DC-T-CCR7+/+ mice, expressing CCR7 on T cells and DCs, show normal frequencies of LN T cells and regular architecture of the T cell zone, and (3) adoptively transferred T cells egress more quickly from LNs of T-CCR7+/+ than from wild-type recipients under steady state, noninflammatory conditions. It is still not entirely clear how DCs affect the dwell time of T cells but data provided here would suggest that the CCL21-CCR7 axis is involved. A recent study failed to detect CCL21 mRNA in LN DCs in mice, rendering the possibility unlikely that DCs serve as a direct source for CCL21 (Link et al., 2007). Showing that TRCs in vivo express elevated levels of CCL21 mRNA in the presence of DCs and that CCL21 can bind to the surface of DCs independent of the presence of CCR7, our data would support a model in which DCs promote CCL21 production by TRCs and potentially help to "present" it to other cells such as T cells. However, we cannot rule out that other cells than DCs expressing CCR7 are also involved in maintaining LN homeostasis. We could recently demonstrate that mouse pDC are strongly reduced in Ccr7-deficient mice and that pDCs express very low levels of Ccr7 (Seth et al., 2011). On the basis of this very weak expression of the endogenous Ccr7, we expectedly failed to reveal expression of human CCR7 on pDCs once Cd11c-cre+ mice had been crossed in. Because DC-T-CCR7+/+ mice also showed close to normal pDC counts, further studies have to clarify a potential role for pDCs in LN homeostasis. Another important cell population that expresses Ccr7 is LTi cells, which are known to express CD4 in mice (Mebius et al., 1997). When comparing the expression levels of human CCR7 in the T-CCR7+/+ mice with that of mouse Ccr7 reported earlier on LTi cells (Ohl et al., 2003), we found similarly low levels. It was thus unexpected to observe reduced numbers of LTi cells in T-CCR7+/+ mice but not in CCR7stop/stop or DC-T-CCR7+/+ mice. Given that we found a strong variation in the number of LTi cells within individual LNs of all genotypes, we think that it is rather unlikely that reduced numbers of LTi cells contribute to LN homeostasis. Yet we can currently not exclude this possibility. Furthermore, we can also not rule out the possibility that lack of sDCs affect the integrity of the lymphatic endothelial cells lining the medullary and cortical sinuses, which in turn could allow a more rapid egress of T cells.

A central role for DCs has been recently reported for the initiation and maintenance of induced bronchus-associated lymphoid tissue (iBALT) (GeurtsvanKessel et al., 2009; Halle et al., 2009). Of interest, signaling through the lymphotoxin beta receptor (LT β -R) seems to play an essential role in this process given that delivery of a soluble LT β -R led to the disintegration of iBALT. In this context, it is also noteworthy to mention that LT β -R signaling has been identified to be essential for HEV formation and maintenance (Browning et al., 2005). Thus, it seems possible that LT β R signaling in DCs could be involved in HEV formation potentially via VEGF production.

We and others could recently reveal that CCL21 provides strong haptokinetic stimuli to T cells (Huang et al., 2007; Okada and Cyster, 2007; Worbs et al., 2007). Thus, decreased levels of CCL21 could influence the migration behavior, in particular of such T cells moving during random walk toward cortical or medullary sinusoids where they would be exposed to an egress-promoting S1P gradient. In this model, promigratory CCR7 signals would keep T cells on the TRC network, thus making them less susceptible to react to the S1P₁-mediated egress signal. A similar effect might be exerted by increased scanning activity on DCs displayed by T cells in the presence of CCR7 ligands (Friedman et al., 2006). Once CCR7 is less well triggered because of reduced availability of CCL21 in the T cell area, T cells might be less efficiently retained and, consequently, possess a higher propensity to leave the LNs via efferent lymphatics. This model is supported by Cyster and colleagues showing that Ccr7-deficient T lymphocytes egress more quickly from LNs than wild-type T cells (Pham et al., 2008) and is also in line with previous studies from our group showing that Ccr7-deficient B cells are not retained within the T cell zone but rapidly move to B cell follicles (Förster et al., 1999).

Interestingly, applying in vivo two-photon microscopy studies, we and others reported earlier that in all situations in which either CCR7 or its ligands were missing, T cells migrated with reduced directionality and velocity (Huang et al., 2007; Okada and Cyster, 2007; Worbs et al., 2007), suggesting that CCR7 ligands might help to retain T cells on the TRCs network as originally described in a pivotal study by Germain and colleagues (Bajénoff et al., 2006)

Furthermore, we could recently show that naive T cells home to LNs not only via HEVs but also via afferent lymphatic vessels. Although both wild-type and Ccr7-deficient T cells entered the LN via the peripheral medullary sinus after intralymphatic injection only wild-type, but not Ccr7^{-/-}, T cells were able to migrate from the medullary cord into the deep LN paracortex (Braun et al., 2011). Wild-type T cells migrate into the LN paracortex probably by following a gradient of immobilized CCL21 or CCL19, which serves as another ligand for CCR7. In the present study, we did not address a potential role for the latter chemokine in LN T cell homeostasis. This was primarily due to the fact that we were not able to detect staining of CCL19 on LN sections with the reagents currently available (data not shown). Thus, we cannot formally exclude that CCL19 contributes to the homeostasis of T cells in LN. However, on the basis of studies using Cc/19-deficient mice that show regular LN architecture and normal T cell counts in LNs (Link et al., 2007), it seems likely that CCL21 rather than CCL19 might be the key player in CCR7-mediated LN homeostasis.

Dendritic Cells and T Cell Homeostasis



In summary, data presented here reveal an important role for steady state-trafficking DCs in LN T cell homeostasis. They positively affect the development of HEVs and thus the T cell homing capacity to LNs. Furthermore, DCs affect the production of CCL21 in LNs and promote its "presentation," thereby prolonging the dwell time of T cells within LNs.

EXPERIMENTAL PROCEDURES

Animals

Mice were bred at the central animal facility of Hannover Medical School under specific pathogen-free conditions or purchased from Charles River. The following mouse strains were used: C57BL/6; B6.129P2(C)-Ccr7^{tm1Rfor}/J ¹, backcrossed on C57BL/6 for >15 generations (designated Ccr7^{-/-}); B6.Cg-Tg(Cd4-cre)1Cwi (designated Cd4-cre³); B6.Cg-Tg(ltgax-cre)1-1Reiz/J (designated Cd11c-cre³); B6.Sv129-Rag2^{tm1} (designated Rag2^{-/-}); and C57BL/6-rosa26^(SA-CrepA) (designated germline deleter). All animal experiments have been approved by the institutional review board and local authorities.

Humanized CCR7 Mice

A detailed description of the conditional humanized CCR7-proficient mice can be found in the Supplemental Information.

Antibodies

The following antibodies and conjugates were used in this study: rat anti-human CCR7 mAb (clone 3D12), rat anti-mouse CCR7 (clone 4B12), anti-CD4-PerCp, anti-MHCII(I-A^b), anti-CD11c-biotin, anti-Meca79 (BD Biosciences), anti-CD19-FITC (Southern Biotechnologies), anti-CD62L-PE, anti-CD117-PE (Caltag), and anti-CD31-PE (PharMingen). Anti-CD3 (clone 17A2), anti-B220-Cy3 (clone TIB 146), anti-IgD (clone HB250), and anti-CD8-FITC (clone RM CD8) antibodies were produced in our laboratories. Biotinylated antibodies were recognized by streptavidin coupled to Alexa°488 (Molecular Probes). Unconjugated anti-human and anti-mouse CCR7 antibodies were revealed by mouse anti-rat-Cy5 (Jackson Laboratories). FITC-, Cy3-, and Cy5-conjugates of anti-IgD, anti-CD3, and anti-CD8b antibodies were prepared as recommended by the manufacturer (Amersham).

Flow Cytometry

LNs and spleen were minced through a nylon mesh and washed with PBS supplemented with 3% FCS. Erythrocytes of blood and spleen were lysed with a buffer containing ammonium chloride (1.7 M), potassium hydrogen carbonate (100 mM), and EDTA (1 mM). For LN preparation containing endothelial and stromals cells, LNs were treated with 564 U/ml collagenase type 2 (Worthington Biochemical) + 40 $\mu g/ml$ DNase I (Sigma-Aldrich) for 30 min at $37^{\circ} C$. The cell suspension was resuspended 40 times with a Pasteur pipette. EDTA was added to a final concentration of 10 mM EDTA. After passing cell suspension through a 70 μm filter, cells were stained with antibodies as described above and analyzed with a FACSCalibur or LSRII (BD Biosciences).

Immunohistology and Measurement of High Endothelial Venule Length

Organs were embedded in OCT and 8 μm cryosections were cut. Sections were air-dried and fixed in ice-cold acetone for 10 min and stained with indicated antibodies as described earlier (Pabst et al., 2005). Slides were analyzed with an Axiovert 200M microscope and Axiovision software (Carl Zeiss) or an IX81 microscope and analySIS^D software (Olympus). HEV length and LN section area was calculated with ImageJ software.

In Vitro Differentiation and Transfer of DCs

A total of 2 × 10⁶ bone marrow cells from tibia and femur of mice were cultured in RPMI 1640, 10% FCS, β -ME, glutamine, and penicillin/streptomycin supplemented with 100–200 ng/ml GM-CSF produced by a recombinant cell line for 8 days. In some experiments, cells were matured for 2 additional days with 1 µg/ml PGE2 (Sigma-Aldrich) and 30 ng/ml TNF- α (PeproTech). For DC transfer, semimature BMDCs were gathered at day 8, labeled with 5µM CFSE;

subsequently, 1 to 3 \times 10 6 BMDCs were injected s.c. in the femoral leg, the flank of the mice, or the footpad.

Binding of CCL21 to DCs

We incubated 5 \times 10 5 to 1 \times 10 6 in vitro differentiated DCs in 100 ml with 250 ng murine CCL21 (R&D Systems) for 30 min. Cells were washed twice in PBS and blocked with 1% BSA in PBS containing Fc-block (diluted 1:100; BD Biosciences) for 15 min. Rabbit anti-CCL21 (PeproTech,) diluted to 1 $\mu g/ml$ in PBS was incubated for 30 min; cells were washed twice in PBS before anti-rabbit PE secondary antibody (Jackson ImmunoResearch) was incubated for 30 min. Alternatively, we used a goat-anti-CCL21 (R&D Systems) Ab, which was revealed by a biotinylated donkey-anti-goat antibody (Jackson) and then by streptavidin-PerCP (BD Biosciences). In some experiments, NaClO $_3$ was added to the BMDCs cultures at 50–75 μ M 3 and 1 day prior staining with CCL21. Presence of endogenous CCL21 on LN DCs was revealed as described for BM DCs.

Chemotaxis Assay and In Vitro Inhibition

We resuspended 1 × 10^6 splenic cells or in vitro differentiated BMDCs in $100~\mu$ l RPMI and loaded them in collagen-coated transwells (Corning BV, $5~\mu$ m pore size) that were placed in 24-well plates containing $400~\mu$ l medium or medium supplemented with 100~nM to 300~mM CCL21. After incubation for 3~hr at 37° C, cells migrated were collected, counted, and stained with mAb for determining the number of migrated T cells by flow cytometry.

Skin Painting

The skin of the ears was painted two times with 0.1% Fluoresceinisothiocyanate (FITC) in acetone/dibutylphthalate (1:1). Twenty-four hours later, the mice were sacrificed, the facial LNs were isolated, and single-cell suspensions were prepared. The frequency of cells positive for CD11c, MHC II, and FITC were determined by flow cytometry.

In Vivo Migration

Splenic lymphocytes were isolated as described above. We preincubated 2×10^6 cells/ml at $37^\circ C$ for 30 min in RPMI 1640 containing 5% FCS, incubated them with 5 μM CFSE or TAMRA for 10 min at $37^\circ C$, and washed them in ice-cold PBS with 3% FCS. We mixed 5×10^6 cells of each color and i.v. transferred them into the tail vein of recipients. Three hours later, mice were sacrificed and lymphocytes were isolated from different organs. The ratio or total number of recovered CFSE- and TAMRA-labeled T cells was determined by flow cytometry. Ratios obtained were corrected for the ratio present in the injected mixtures. For analyzing the location of T cells in relation to HEV position T cells of C57BL/6 donors were enriched by MACS-sorting with biotinylated anti-B220 mAb and streptavidin beads (Miltenyi). A total of 1 \times 10 6 TAMRA-labeled T cells were i.v. transferred in C57BL/6 wild-type and T-CCR7+/+ recipients. Mice were sacrificed; the LNs were isolated and frozen in OCT.

Stable Bone Marrow Chimeras

Bone marrow was prepared from femurs and tibiae of T- $CCR7^{+/+}$ and $Rag2^{-/-}$ mice and then separated on Lympholyte M. Recipients for bone marrow transplantation were 6- to 8-week-old sex-matched T- $CCR7^{+/+}$ mice. Before transplantation, adult recipient mice were lethally irradiated (5 Gy) twice at an interval of 4 hr. Approximately 1.5×10^7 bone marrow cells were transferred to irradiated recipients. For mixed chimeras, 80% $Rag2^{-/-}$ and 20% T- $CCR7^{+/+}$ bone marrow were mixed before transplantation. Control animals received 100% T- $CCR7^{+/+}$ bone marrow cells. Three to four weeks later, chimeras were shaved and UV irradiated for 30 min. UV irradiation mobilizes DCs of the skin and their progenitors to allow for replacement of these cells. Chimeric mice were analyzed 11-12 weeks after transplantation.

Treatment with Blocking Antibodies

To block homing of lymphocytes to LNs mice received each i.p. and i.v. 125 μg anti-L-selectin (clone MEL-14).

Real-Time PCR

RNA was isolated from cells via the Absolutely RNA Microprep Kit (Stratagene) and converted into cDNA (Superscript II reverse transcriptase, Invitrogen) with



random hexamer primers. Quantitative PCR was performed on a Lightcycler 2.0 (Roche) with the SYBR Premix Ex Taq Kit (Takara). The primers used are listed in the Supplemental Information.

Isolation of FRCs

Inguinal, axillary, brachial, and popliteal LNs were pooled from mice, mechanically disrupted, and digested with Liberase (Roche). CD45.2-positive cells were removed by MACS. The remaining cells were stained with antibodies to gp38, CD24 and CD45.2, and Dapi. CD45.2 negative, gp38⁺ CD24⁻ DAPI⁻ cells were sorted. Greater than 97% of the sorted cells were CD45.2⁻ with more than 85% of these cells expressing gp38.

SUPPLEMENTAL INFORMATION

Supplemental Information includes two figures and Supplemental Experimental Procedures and can be found with this article online at doi:10.1016/j. immuni.2011.10.017.

ACKNOWLEDGMENTS

We thank I. Prinz for scientific discussions and G. Bernhardt for critically reading the manuscript. We thank W. Müller, Manchester, and B. Reizis, New York City, for providing *Cd4-cre* and *Cd11c-cre* mice, respectively. This work was supported by a Deutsche Forschungsgemeinschafts grants SFB621-A1 and SFB587-B3 to R.F. and Nycomed GmbH. A.H. is employee of Nycomed GmbH (Konstanz, Germany).

Received: December 5, 2008 Revised: September 16, 2011 Accepted: October 25, 2011 Published online: December 22, 2011

REFERENCES

Bajénoff, M., Egen, J.G., Koo, L.Y., Laugier, J.P., Brau, F., Glaichenhaus, N., and Germain, R.N. (2006). Stromal cell networks regulate lymphocyte entry, migration, and territoriality in lymph nodes. Immunity *25*, 989–1001.

Banchereau, J., and Steinman, R.M. (1998). Dendritic cells and the control of immunity. Nature 392, 245–252.

Braun, A., Worbs, T., Moschovakis, G.L., Halle, S., Hoffmann, K., Bölter, J., Münk, A., and Förster, R. (2011). Afferent lymph-derived T cells and DCs use different chemokine receptor CCR7-dependent routes for entry into the lymph node and intranodal migration. Nat. Immunol. 12, 879–887.

Browning, J.L., Allaire, N., Ngam-Ek, A., Notidis, E., Hunt, J., Perrin, S., and Fava, R.A. (2005). Lymphotoxin-beta receptor signaling is required for the homeostatic control of HEV differentiation and function. Immunity *23*, 539–550.

Campbell, J.J., Bowman, E.P., Murphy, K., Youngman, K.R., Siani, M.A., Thompson, D.A., Wu, L., Zlotnik, A., and Butcher, E.C. (1998). 6-C-kine (SLC), a lymphocyte adhesion-triggering chemokine expressed by high endothelium, is an agonist for the MIP-3beta receptor CCR7. J. Cell Biol. *141*, 1053–1059.

Chyou, S., Ekland, E.H., Carpenter, A.C., Tzeng, T.C., Tian, S., Michaud, M., Madri, J.A., and Lu, T.T. (2008). Fibroblast-type reticular stromal cells regulate the lymph node vasculature. J. Immunol. *181*, 3887–3896.

Cyster, J.G. (2005). Chemokines, sphingosine-1-phosphate, and cell migration in secondary lymphoid organs. Annu. Rev. Immunol. 23, 127–159.

Förster, R., Schubel, A., Breitfeld, D., Kremmer, E., Renner-Müller, I., Wolf, E., and Lipp, M. (1999). CCR7 coordinates the primary immune response by establishing functional microenvironments in secondary lymphoid organs. Cell 99, 23–33.

Friedman, R.S., Jacobelli, J., and Krummel, M.F. (2006). Surface-bound chemokines capture and prime T cells for synapse formation. Nat. Immunol. 7, 1101–1108

GeurtsvanKessel, C.H., Willart, M.A., Bergen, I.M., van Rijt, L.S., Muskens, F., Elewaut, D., Osterhaus, A.D., Hendriks, R., Rimmelzwaan, G.F., and

Lambrecht, B.N. (2009). Dendritic cells are crucial for maintenance of tertiary lymphoid structures in the lung of influenza virus-infected mice. J. Exp. Med. 206. 2339–2349.

Halle, S., Dujardin, H.C., Bakocevic, N., Fleige, H., Danzer, H., Willenzon, S., Suezer, Y., Hämmerling, G., Garbi, N., Sutter, G., et al. (2009). Induced bronchus-associated lymphoid tissue serves as a general priming site for T cells and is maintained by dendritic cells. J. Exp. Med. 206, 2593–2601.

Hintzen, G., Ohl, L., el Rio, M.L., Rodriguez-Barbosa, J.I., Pabst, O., Kocks, J.R., Krege, J., Hardtke, S., and Förster, R. (2006). Induction of tolerance to innocuous inhaled antigen relies on a CCR7-dependent dendritic cell-mediated antigen transport to the bronchial lymph node. J. Immunol. *177*, 7346–7354.

Huang, J.H., Cárdenas-Navia, L.I., Caldwell, C.C., Plumb, T.J., Radu, C.G., Rocha, P.N., Wilder, T., Bromberg, J.S., Cronstein, B.N., Sitkovsky, M., et al. (2007). Requirements for T lymphocyte migration in explanted lymph nodes. J. Immunol. *178*, 7747–7755.

Humphries, D.E., and Silbert, J.E. (1988). Chlorate: A reversible inhibitor of proteoglycan sulfation. Biochem. Biophys. Res. Commun. *154*, 365–371.

Link, A., Vogt, T.K., Favre, S., Britschgi, M.R., Acha-Orbea, H., Hinz, B., Cyster, J.G., and Luther, S.A. (2007). Fibroblastic reticular cells in lymph nodes regulate the homeostasis of naive T cells. Nat. Immunol. *8*, 1255–1265.

Lohr, J., Knoechel, B., Nagabhushanam, V., and Abbas, A.K. (2005). T-cell tolerance and autoimmunity to systemic and tissue-restricted self-antigens. Immunol. Rev. 204, 116–127.

Martin-Fontecha, A., Sebastiani, S., Höpken, U.E., Uguccioni, M., Lipp, M., Lanzavecchia, A., and Sallusto, F. (2003). Regulation of dendritic cell migration to the draining lymph node: Impact on T lymphocyte traffic and priming. J. Exp. Med. 198. 615–621.

Mebius, R.E., Streeter, P.R., Brevé, J., Duijvestijn, A.M., and Kraal, G. (1991). The influence of afferent lymphatic vessel interruption on vascular addressin expression. J. Cell Biol. *115*, 85–95.

Mebius, R.E., Rennert, P., and Weissman, I.L. (1997). Developing lymph nodes collect CD4+CD3- LTbeta+ cells that can differentiate to APC, NK cells, and follicular cells but not T or B cells. Immunity 7, 493–504.

Ohl, L., Henning, G., Krautwald, S., Lipp, M., Hardtke, S., Bernhardt, G., Pabst, O., and Förster, R. (2003). Cooperating mechanisms of CXCR5 and CCR7 in development and organization of secondary lymphoid organs. J. Exp. Med. 197. 1199–1204.

Ohl, L., Mohaupt, M., Czeloth, N., Hintzen, G., Kiafard, Z., Zwirner, J., Blankenstein, T., Henning, G., and Förster, R. (2004). CCR7 governs skin dendritic cell migration under inflammatory and steady-state conditions. Immunity *21*, 279–288.

Okada, T., and Cyster, J.G. (2007). CC chemokine receptor 7 contributes to Gi-dependent T cell motility in the lymph node. J. Immunol. 178, 2973–2978.

Pabst, O., Herbrand, H., Worbs, T., Friedrichsen, M., Yan, S., Hoffmann, M.W., Körner, H., Bernhardt, G., Pabst, R., and Förster, R. (2005). Cryptopatches and isolated lymphoid follicles: Dynamic lymphoid tissues dispensable for the generation of intraepithelial lymphocytes. Eur. J. Immunol. 35, 98–107.

Pappu, R., Schwab, S.R., Cornelissen, I., Pereira, J.P., Regard, J.B., Xu, Y., Camerer, E., Zheng, Y.W., Huang, Y., Cyster, J.G., and Coughlin, S.R. (2007). Promotion of lymphocyte egress into blood and lymph by distinct sources of sphingosine-1-phosphate. Science *316*, 295–298.

Pham, T.H., Okada, T., Matloubian, M., Lo, C.G., and Cyster, J.G. (2008). S1P1 receptor signaling overrides retention mediated by G alpha i-coupled receptors to promote T cell egress. Immunity 28, 122–133.

Rosen, H., Sanna, M.G., Cahalan, S.M., and Gonzalez-Cabrera, P.J. (2007). Tipping the gatekeeper: S1P regulation of endothelial barrier function. Trends Immunol. 28, 102–107.

Sackstein, R. (2005). The lymphocyte homing receptors: Gatekeepers of the multistep paradigm. Curr. Opin. Hematol. 12, 444–450.

Seth, S., Oberdörfer, L., Hyde, R., Hoff, K., Thies, V., Worbs, T., Schmitz, S., and Förster, R. (2011). CCR7 essentially contributes to the homing of plasmacytoid dendritic cells to lymph nodes under steady-state as well as inflammatory conditions. J. Immunol. *186*, 3364–3372.

Immunity

Dendritic Cells and T Cell Homeostasis



Steinman, R.M., Hawiger, D., and Nussenzweig, M.C. (2003). Tolerogenic dendritic cells. Annu. Rev. Immunol. 21, 685-711.

von Andrian, U.H., and Mackay, C.R. (2000). T-cell function and migration. Two sides of the same coin. N. Engl. J. Med. 343, 1020–1034.

von Andrian, U.H., and Mempel, T.R. (2003). Homing and cellular traffic in lymph nodes. Nat. Rev. Immunol. 3, 867–878.

Webster, B., Ekland, E.H., Agle, L.M., Chyou, S., Ruggieri, R., and Lu, T.T. (2006). Regulation of lymph node vascular growth by dendritic cells. J. Exp. Med. 203, 1903-1913.

Worbs, T., Mempel, T.R., Bölter, J., von Andrian, U.H., and Förster, R. (2007). CCR7 ligands stimulate the intranodal motility of T lymphocytes in vivo. J. Exp. Med. 204, 489-495.